JOURNAL OF MATERIALS SCIENCE 13 (1978) 1151–1176

Review
Infra-red transmitting materials

Part 1 *Crystalline materials*

I. W. DONALD*, P. W. McMILLAN
Department of Physics, University of Warwick, Coventry, UK

Infra-red transparent crystalline ceramic materials, primarily for application in the 1 to 6 μm spectral range, are reviewed with reference to existing materials and fabrication techniques. Relationships between infra-red transmission and various physical and mechanical properties are also discussed, and an attempt is made to suggest methods by which (i) existing materials might be improved, and (ii) the performance of new materials might be predicted.

1. Introduction

Infra-red transmitting materials are required for a number of diverse applications ranging from infra-red lenses and related optical components, to windows and domes that may function primarily to protect detecting systems from the environment. For some applications, including infra-red laser components, transmission approaching 100% is essential in the desired wavelength range in order to prevent heating and subsequent distortion or even melting of the components, whilst for other uses, including camera lenses, protecting windows and domes etc., transmission significantly less than 100% may often be tolerated. Depending on the primary application other properties may also be important, including mechanical strength and toughness, mechanical and thermal shock resistance, thermal and chemical stability, and rain-erosion resistance.

The survey commences with a consideration of the theoretical aspects associated with both infra-red transmission and mechanical and physical properties of materials. This is then related to methods which may be suitable for improving mechanical properties whilst retaining acceptable infra-red transmission. A comprehensive literature survey of existing materials and fabrication techniques then follows, and relationships between the mechanical and physical properties and the infra-red transmission are established on a semi-empirical basis.

2. Theoretical considerations

2.1. Infra-red transmission

The proportion of incident radiation transmitted by a material is a function of absorption and scattering within the bulk of the material, and of reflection at the external surfaces. The intensity of transmitted radiation, I_t, through a sample of thickness t, may be estimated from the Lambert–Bouger law:

$$I_t = I_i \exp^{-\alpha t} \quad (1)$$

where the intensity of the incident radiation is I_i, α is the absorption coefficient, and reflection losses at the surfaces are neglected.

If reflection at the two interfaces is taken into account, the ratio of transmitted to incident intensity, I_t/I_i, is given by:

$$I_t/I_i = (1-R)^2 e^{-\alpha t} \quad (2)$$

where R, the reflectivity at normal incidence, is dependent on the refractive index n, of the material, and for reflection by a transparent medium in air is given by:

$$R = \frac{(n_\lambda - n_{air})^2 + K_{air}^2}{(n_\lambda + n_{air})^2 + K_{air}^2} \quad (3)$$

*Now with the Department of Metallurgy, University of Sheffield, Sheffield, UK.

where K, the extinction coefficient $= \lambda\alpha/4\pi n$

For air, $\alpha \sim 0$, $\therefore K \sim 0$, and also, $n_{air} \sim 1.0$, hence:

$$R \sim \left(\frac{n_\lambda - 1}{n_\lambda + 1}\right)^2 \tag{4}$$

and:

$$\frac{I_t}{I_i} \sim \left\{1 - \left(\frac{n_\lambda - 1}{n_\lambda + 1}\right)^2\right\} e^{-\alpha t} \tag{5}$$

The value of α can be calculated from transmittance data, T_1 and T_2, on two samples of thicknesses, t_1 and t_2. Hence:

$$T_1 = (1-R)^2 e^{-\alpha t_1}$$

$$T_2 = (1-R)^2 e^{-\alpha t_2}$$

and

$$\alpha = \frac{\ln T_1 - \ln T_2}{t_2 - t_1} \tag{6}$$

Absorption of incident radiation is due to a combination of mechanisms, both intrinsic and extrinsic, and this is discussed below.

2.1.1. Intrinsic absorption mechanisms

2.1.1.1. Short wavelength cut-on. Absorption at short wavelengths is due to electronic transitions between electron states and is a function of the energy gap, E_g, of the material. Materials which do not exhibit an energy gap (e.g. metals which may have overlapping valence and conduction bands, or in which the highest occupied band is only partly filled) will absorb incident electromagnetic radiation over a wide frequency range, and when in significant thicknesses they will be opaque (e.g. aluminium film 40 Å thick deposited on a transparent substrate will transmit 65% of incident radiation of wavelength 0.4 μm, whilst only 0.4% will be transmitted when the thickness is increased to 400 Å [1]).

For insulators and semiconductors, the wider the energy gap, the shorter will be the wavelength of the cut-on (i.e. the greater the energy required to promote an electronic transition). Hence, depending on the value of E_g, the cut-on may occur in the ultra-violet, in the visible, or in the infra-red.

The short wavelength cut-on, λ_c is given by the relationship:

$$\lambda_c = hc/E_g \tag{7}$$

And for E_g in eV, $\lambda_c = 1.24/E_g$.

The energy gap is dependent on temperature (and to a lesser extent on hydrostatic pressure), and at a temperature T_1, the energy gap, $E_g(T)$, may be expressed as a function of temperature by:

$$E_g(T) = E_g - \beta T \tag{8}$$

where E_g is the energy gap at a given reference temperature, and β is the temperature coefficient, which may take values typically of the order of 10^{-4} eV K^{-1}.

2.1.1.2. Long wavelength cut-off. The long wavelength cut-off is due to infra-red active lattice absorption, and depends on the vibrational modes of the atoms or ions of the material. Vibrations of large amplitude will occur when incident radiation is of the same frequency as the resonant frequency of vibration of the ions in the crystal, but for electromagnetic radiation to excite vibrational modes, the molecule must possess a permanent dipole moment which can be activated by the oscillating electric field of the incident radiation. This first order effect occurs in ionic crystals only, and is known as reststrahlen ("residual ray") absorption.

Vibrations of linear non-polar molecules, (i.e. O_2, N_2 etc.), cause no change in electric moment and hence these molecules would not be expected to exhibit infra-red vibrational spectra. However, absorption may be observed under certain conditions due to induced dipole moments resulting from distortion of molecules upon collision. Similarly, a non-ionic crystal can have an effective charge, and consequently a dipole moment, if the atoms are not identical, and induced dipole moments may also be possible in elemental materials such as diamond and silicon. Although such homopolar materials do not possess a permanent dipole moment, one vibrational mode (which is infra-red inactive) may induce charges on the atoms, and a second mode may simultaneously cause a vibration of the induced charges, so producing an electric moment of the second order, and hence coupling to the field of the incident radiation.

The absorption coefficient for these second order effects is generally several orders of magnitude lower than restrahlen absorption, but may still effectively render a material opaque over a given wavelength region, when in useful thickness. When the absorption coefficient is very high,

broadening of the absorption band may also be so severe as to render the material opaque over a wide wavelength range.

The simplest mode of vibration of a linear diatomic molecule consisting of two point masses, m_1 and m_2, is a simple harmonic oscillation of the two masses along the line joining them. This is the classical description of a linear polar diatomic molecule, and the frequency of the vibration, according to this model is given by:

$$\bar{\nu} = (1/2\pi)(f/\mu)^{1/2} \quad (9)$$

where the reduced mass, $\mu = [m_1 m_2/(m_1 + m_2)]$ and f is the restoring force, or "force constant".

Such a simple equation is very effective in predicting the fundamental absorption frequency of many polar diatomic molecules, as well as some multi-atomic systems, and even some homopolar systems, and this is considered in more detail later.

In Classical mechanics, the oscillator could take any value of energy depending only on the value of the amplitude of the vibration. However, for an atomic system, the energy is variable only in quantized increments of $h\nu$, where ν is the wavenumber of the vibration. Hence, for a harmonic oscillator, absorptions are allowed only for values $\Delta v = \pm 1$, where v is the vibrational quantum number of the atomic system. As with the Classical case, the initial state of the system is immaterial and for each transition, radiation of the same frequency is emitted or absorbed, independent of the degree to which the vibration is excited.

When the more realistic case of an anharmonic oscillator is considered, in addition to the fundamental frequency, a series of vibrational bands arises which can be characterized by specifying additional vibrational quantum states, $\Delta v = \pm 2$, ± 3 etc. The frequency of the ± 2 band is approximately double that of the fundamental band, and is known as an overtone, or harmonic. Higher overtones occur with rapidly decreasing probability, and the long wavelength limit may often be set by the first overtone of the fundamental.

For molecules containing more than two ions there will be additional normal modes of vibration. For simple oscillatory motions in which all atoms undergo their maximum displacements at the same time, and pass through their equilibrium positions at the same time, there are $(3n - 5)$ or $(3n - 6)$ genuine normal modes of vibration, depending on whether the system is linear or not (where n = number of atoms in the system). The 5 or 6 non-genuine vibrations are simply translations or rotations of the molecule as a whole.

In still more complex molecules, for which a greater number of independent vibrations are possible, degenerate vibrations may also exist, due to symmetry considerations, when two or more normal modes have the same frequency of vibration. Other vibrations may coincidentally exhibit nearly identical frequencies, and interaction between such states can result in two mixed absorptions which may differ significantly in frequency from each other, and hence from the expected bands. The effect of such factors obviously increases as the complexity of the molecule increases. Additional complications also arise due to environmental factors such as coupling between individual molecular units.

One method by which the vibrational frequencies of molecules may be determined is the Wilson FG matrix technique [2]. This is employed to find the equations of motion of vibrating molecules from a knowledge of the geometrical arrangement of the atoms within the molecule. Another approach is to employ the Kramers–Krönig relationships to obtain the optical constants from reflectivity measurements [3].

Various simplified approaches have been taken in attempts to predict theoretically the absorptions associated with given materials. Absorption frequencies may be calculated on the basis of simple fundamental molecular units whose characteristic frequencies are assumed not to vary with their position in the molecule, or somewhat more realistically, it may be assumed that the units are linked to fixed walls which represent the rest of the structure. Hence, a crystalline solid A_xB_yO, may be considered to be composed of AO_p and BO_r sub-groups. There is obviously some interaction between vibrations associated with the separate groups, but generally a rigorous treatment is impossible due to the mathematical complexity involved.

For instance, Mackenzie [4] found good agreement between the predicted frequencies of ideal mullite ($3Al_2O_3 \cdot 2SiO_2$) and the experimentally obtained value by assuming the compound to be based on discrete tetrahedral and octahedral Al–O units and tetrahedral Si–O units. Similarly, O'Horo *et al.* [5] considered Al–O octahedra and Mg–O tetrahedra in $MgAl_2O_4$

spinel, and found reasonable agreement between the theoretical values and the experimental data.

It is clear that the vibration of a given unit, A–O, is strongly dependent upon the co-ordination number. For instance, the change in co-ordination of Si from tetrahedral in quartz to octahedral in stishovite is accompanied by a shift of the main absorption band from the 8.33 to the 10.00 μm region. Similar shifts are observed for change in co-ordination of other materials, and the characteristic absorption regions of some co-ordinated groups are summarized in Table I.

2.1.2. Extrinsic absorption mechanisms

Absorption or scattering of incident radiation may occur due to impurities in the matrix, including solid solutions or second-phase inclusions, or due to other factors which may produce inhomogeneity, including grain boundaries or dislocation networks, and local variations in composition, density etc.

2.1.2.1. Electronic absorption. This may occur due to the donation of free carriers by dissolved impurity atoms. The effect is particularly prevalent for semiconductors which exhibit small energy gaps, and effectively such impurities displace the short wavelength cut-on of the material.

2.1.2.2. Vibrational absorption. Absorption may occur due to fundamental vibrations exhibited by second-phase inclusions, or due to vibrations between bound impurity–matrix states. For instance, H_2O in the form of entrapped molecular water or as bound hydroxyl groups can affect the transmission of many materials.

TABLE I Characteristic absorption ranges of some co-ordinated groups.

Cation A	Characteristic absorption range (μm)			
	Isolated units		Interconnected units	
	AO_4	AO_6	AO_4	AO_6
Si	9.5–12.5	–	8.3–10.0	10.5–11.1
Ge	11.8–14.7	< 20	⩽ 11.1	⩽ 14.3
Ti	12.5–14.5	< 20	–	16.7–20.0
Al	12.5–15.4	20–25	11.5–14.3	⩽ 15.4
Fe(III)	15.4–18.2	25.0–33.3	14.3–18.2	18.2–25.0
Cr(III)	–	22.2–33.3	–	⩽ 15.4
Ga	14.3–17.5	~ 25	13.3–16.7	16.7–20.0
Zn	20–22.2	–	16.7–25.0	–
Mg	16.7–20.0	–	–	⩽ 20.8
Fe(II)	~ 22.2	–	–	~ 31.3
Mn(II)	~ 22.2	–	–	~ 31.3
Li	20–25	–	16.7–25.0	–

2.1.2.3. Scattering. Scattering involves the absorption and simultaneous re-emission of incident radiation, and unless the material is homogeneous the effect can be very significant. Scattering may be caused by the presence of second-phase inclusions and porosity, grain boundaries and dislocation networks, local fluctuations in composition or density, and the effects of anisotropy in refractive index.

It can be shown that the angular intensity distribution of radiation scattered by second-phase inclusions which are small compared to the wavelength of the incident radiation (Rayleigh scattering) is of the form:

$$I(\theta) = \left(\frac{1 + \cos^2\theta}{x^2}\right) \frac{8\pi^4}{\lambda^4} r^6 \left|\frac{N^2 - 1}{N^2 + 2}\right|^2 I_0 \quad (10)$$

where $I(\theta)$ is the specific intensity at the scattering angle θ, x is the distance from the scattering centre, r is the radius of the inclusion, N is the ratio of refractive indices of inclusion and medium, and I_0 is the incident intensity.

Assuming $\Delta n > 0$, the intensity of the scattered radiation at any given angle therefore varies directly as r^6/λ^4, and for minimal scattering either the refractive indices of medium and dispersion should be matched, or the dispersoid size should be significantly less than that of the wavelength of the incident radiation; either of these conditions is sufficient in itself.

In the case of scattering by particles which are of the same order of size as the wavelength of the incident radiation (Mie scattering), the Rayleigh criterion no longer holds, but the important parameters are retained, and for transparency, Δn must approach zero.

The effect of porosity is similar to that of solid inclusions, with the value for the inclusion refractive index approximately equal to unity. It is evident, therefore, that porosity, unless it is of small size, will seriously impede transmission.

For polycrystalline materials grain boundaries may act as scattering centres and thereby affect transmission. In particular, materials of non-cubic symmetry which exhibit significant anisotropy of refractive index generally exhibit high scattering losses. Grain boundaries may also indirectly affect transmission by acting as sinks

for the segregation of large scattering centres including impurity inclusions or pores. In a similar manner diffusion and segregation of impurities to other high-energy lattice sites, including dislocation networks, may also affect transmission. Localized elastic or plastic strains introduced into the matrix due to differential elastic modulii or thermal expansions, or due to coherency strains, may change the value of refractive index locally, and thereby enhance scattering.

Furthermore, matching of refractive indices may be wavelength dependent due to differential dispersion (change of refractive index with wavelength). And finally, surface condition may affect transmission, particularly a rough surface which will significantly increase scattering losses.

2.2. Mechanical and physical properties in relation to infra-red transmission

Assuming a polar bonding component, Equation 9 suggests that the atomic conditions necessary for producing a material of high strength and hardness, high melting temperature, and low thermal expansion, generally run counter to the conditions required for high infra-red transmission. Hence, high transmission is favoured by materials which contain heavy elements interacting by weak force constants, whilst light masses and strong force constants generally favour high strength, high melting point, and low thermal expansion.

The force constant for a diatomic system may be defined as the force required to separate the atoms by unit distance from their equilibrium position, (and hence may be regarded as a measure of the "stiffness" of the bond), and may be related to the elastic modulus, C_{11}, assuming $C_{11}, \gg C_{12}, C_{14}$ etc., by the relationship:

$$f \sim C_{11}\, a,$$

where "a" is the bond length.

Young's modulus, E, for a cubic material is related to the elastic constants by:

$$E \sim \frac{(C_{11} + 2C_{12})(C_{11} - C_{12})}{(C_{11} + C_{12})}, \quad (11)$$

and if

$$C_{11} \gg C_{12}, \quad E \sim C_{11}.$$

Infra-red transmission is hence related to E, and this has important implications when considering the strength of brittle materials. This is considered in more detail in Section 4.

Finally, since $f \sim C_{11}\, a$, it is also evident that the value of the force constant increases with increasing bond length. Consequently, materials with small lattice parameters will generally exhibit better infra-red transmission.

2.3. Strengthening and toughening mechanisms in relation to typical service conditions

Ceramic materials generally exhibit brittle behaviour at ambient temperatures due to a lack of significant stress-relieving mechanisms, and consequently, they are very susceptible to the presence of surface imperfections. In general, brittle materials exhibit very low failure strains, typically $< 0.1\%$, which are relatively insensitive to the value of E. Hence, when considering the feasibility of strengthening infra-red transmitting materials, any mechanism which relies solely on an increase in E will most probably lead to a reduction in infra-red transmission; thus unless a compromise is acceptable, strengthening mechanisms should ideally be aimed at increasing the resistance of the material to crack propagation.

Mechanisms which rely on increasing the resistance to crack propagation are also necessary for promotion of toughness, which is related to work of fracture (defined as the work required per unit area in fracturing a test sample in a controlled manner). Brittle ceramics exhibit very low values for work of fracture, typically of the order of 1 to 100 $J\,m^{-2}$, in contrast to ductile metals, for instance, in which large amounts of energy may be expended in plastic deformation, and which typically yield values of the order of 10^5 to 10^6 $J\,m^{-2}$.

The most appropriate methods of increasing the strength of brittle materials are thermal or chemical techniques which rely on pre-stressing the interface of the material in compression so that a higher strain is required to initiate failure. Particle or fibre-reinforcement or grain-refinement which rely on impeding crack propagation, are also feasible, and these methods have been described elsewhere [6]; however, to be applicable to infra-red transmitting materials careful matching of the components would be essential. Hence, for particle-strengthened systems, either the particle size would have to be significantly less than that of the wavelength of the incident

radiation, which would require mean sizes of the order of 0.1 μm if transmission in the visible is required, or the refractive indices would need to be closely matched. For fibre-reinforcement it would be essential to match the refractive indices.

However, the only effective method of significantly increasing the work of fracture of brittle materials is by fibre-reinforcement. Unfortunately, in addition to the necessary matching of components, the matrix generally microcracks below the ultimate failure stress of the composite, and consequently the high values of work of fracture attainable by fibre-reinforcement may be of limited applicability for infra-red transmitting materials.

An important property related to work of fracture is impact resistance, which is a measure of the energy required to fracture a material under high loading rates, typically $> 1\,\mathrm{m\,sec^{-1}}$. Hence, ceramics exhibit very low resistance to impact, and consequently, any mechanism by which work of fracture is increased can also be expected to lead to a corresponding increase in impact resistance.

A further consideration is thermal shock-resistance, which is a function of both the toughness and the thermal expansion. Due to the low failure strain and low work of fracture of ceramics the stresses encountered during thermal shock are not readily tolerated. For an instantaneous temperature change, ΔT, the thermal strain, ϵ, produced, may be given by:

$$\epsilon = \Delta T \alpha \qquad (12)$$

Hence, assuming a failure strain of 0.1%, a material must exhibit $\alpha \leqslant 4 \times 10^{-6}\,^{\circ}\mathrm{C}^{-1}$ to withstand $\Delta T = 250^{\circ}$ C, and consequently, the only objective answer to this problem is to use materials of low α. However, methods of strengthening by surface manipulation may minimize the effects of thermal shock, and fibre-reinforcement can greatly enhance the resistance, although matrix-microcracking is possible.

Finally, the erosion-resistance is of importance under certain service conditions, including detector-protecting windows and domes encountering dust or rain impact, as in aircraft flight conditions. This is discussed more fully in Section 3.

3. Materials

3.1. Fabrication techniques

3.1.1. Single crystals

Fabrication of single crystals may be divided into solid, melt, or vapour-growth techniques, and will not be discussed in detail, as reviews are available elsewhere [7]. A brief summary of methods applicable to production of infra-red transmitting materials is given below.

Melt growth is feasible by: (a) the Kyropoulis technique in which a cooled seed crystal is brought into contact with a melt, (b) the Czochralski technique in which a seed crystal is gradually withdrawn (usually whilst rotating), after having been allowed to come into contact with a melt, and (c) flux growth, which is analogous to crystal growth from aqueous solution, and involves the use of a high-temperature solvent.

The Czochralski technique is most suited to growth of single crystals for infra-red applications, and the only limitation on the size of crystal obtainable is due to practical considerations. Ideally, a material should exhibit a congruent melting point and a low vapour pressure, although materials of high vapour pressure at the melting point, or which dissociate, may be pulled as single crystals by modified techniques, including compatible liquid-encapsulation. A further interesting modification has been reported in which capillary action is employed to maintain a growing single crystal of virtually any cross-sectional shape above the melt [8]. A die containing capillaries is introduced into the melt, and a single crystal film is formed at the top of the die by introduction of a seed crystal which is subsequently displaced upwards relative to the surface of the die; as the single crystal grows more liquid is transported to the die surface by capillary action. The cross-sectional shape of the crystal is determined by the shape of the die surface, which may contain depressions over which the film is not deposited. Consequently, it is possible to obtain crystals in complex shapes including tubes, rods, and square cross-sections etc., containing channels or holes. The only necessary requirement is that the liquid wets the capillary and the die, and the technique has been successfully employed for growth of Al_2O_3, $MgAl_2O_4$, NaCl, and $LiNbO_3$ using molybdenum dies.

Finally, growth from the vapour phase is also a versatile method for production of single crystals, but is limited by the large number of variables which make it difficult to control adequately. Consequently, it has been most widely employed for the growth of materials which are not readily grown from the liquid-phase, including II–VI

compounds. Basically, for crystal growth to proceed, a substrate surface is kept at a suitable high temperature, and the vapour pressure of the species above the crystal is kept at a value higher than the equilibrium vapour pressure; there will then be a net deposition and crystal growth will proceed. Transport of the species may be instigated by physical or by chemical techniques, which involve direct vaporization from a polycrystalline or amorphous source, or transportation of the individual constituents as more volatile species followed by subsequent reaction, respectively. If separate sources of volatile species are used, the process is usually referred to as chemical vapour deposition (CVD).

3.1.2. Polycrystalline materials

The major problem associated with the production of polycrystalline materials is the requirement for the virtual complete elimination of porosity or impurities which may segregate at grain-boundaries and cause scattering zones. Various methods are available and the most important may be divided into solid-state and vapour-growth techniques.

3.1.2.1. Solid-state techniques: sintering. Sintering is a versatile procedure for preparing a wide variety of components by the heating of compacted powders at temperatures significantly below their melting points, and the major driving force for the sintering process comes from the reduction in the surface area which proceeds as the component densifies. Unfortunately, the retention of residual porosity, and the segregation of impurities at grain boundaries, is a serious problem with materials for optical applications.

Grain-boundary migration, with consequent grain growth and reduction in grain-boundary energy, occurs as sintering progresses. Pores may initially pin grain boundaries, but if the boundary mobility is high, unrestricted migration can lead to entrapment of pores within the grains, which are then difficult to remove, particularly if they contain residual gases which must diffuse away.

Hence, methods of obtaining theoretically dense sintered materials have been directed toward control of grain-boundary mobility so that the initial porosity is maintained within the grain-boundary network which then serves as a sink for the migration of vacancies away from the pores. This may be achieved by the use of certain additives such as a suitable second-phase dispersion, but for optical materials this introduces secondary problems associated with scattering and absorption by the second phase. Homogeneity must therefore usually be maintained, and the solubility limit of the additive (which may work by reducing the grain-boundary energy, and consequently the grain-boundary mobility) must not be exceeded; for instance, $\leqslant 10\,\text{wt}\%\,ThO_2$ has been found very successful in producing theoretically dense Y_2O_3 [9].

In addition to residual porosity, segregation of impurities at grain boundaries can seriously reduce optical transmission, and consequently the initial powders must be of exceptional purity. Powders produced by conventional methods including standard ball-milling etc. are totally inadequate, and various tedious chemical techniques must usually be employed.

For example, in the production of mixed ThO_2–Y_2O_3 powders, co-precipitation of thorium and yttrium oxalates in aqueous solution, followed by drying and calcining to produce finely divided oxides may be employed [10]. The aggregates are then broken down into fine powders by extensive ball-milling in specially adapted mills employing rubber liners and balls of the same material as that to be milled. Gd_2O_3 powders have also been prepared by reacting $Gd(NO_3)_3$ solution with oxalic acid to form the oxalate, and subsequently calcining to form the oxide [11].

Oxides may often be prepared by the general alkoxide process [12] in which a solution of the high purity alkoxide in a suitable solvent such as benzene is reacted with water, i.e.:

$$M(OR)_4 + 2H_2O \xrightarrow[C_6H_6]{} MO_2 + 4ROH$$

where R is an alkyl group.

The metal alkoxide, $M(OR)_4$, may be prepared by reacting the halide, MX_4, with a suitable organic compound, i.e.:

$$MX_4 + 4ROH + 4NH_3 \xrightarrow[C_6H_6]{5^\circ C} M(OR)_4 + 4NH_4X.$$

Mixed oxides may be prepared by employing a mixture of the appropriate alkoxides, and double decomposition is also feasible for the production of certain complex oxides; hence hafnium titanate has been prepared by reacting the appropriate Hf and Ti alkoxides:

$$Hf(OR)_4 + Ti(OR)_4 + 4H_2O \rightarrow HfTiO_4 + 8ROH.$$

$BaTiO_3$ and related compounds have also been prepared as fine powders by co-precipitation of citrates in an alcohol. Elements including Ti, Zr, Nb, Ta, Pb, Sn, Mo, W, Sb, Bi, Ga or La dissolved in citric acid and carbonates or oxides of Mg, Ca, Sr, Ba, Cd dissolved in aqueous formic acid may be co-precipitated by spraying the solutions into an alcohol [13]. In all instances, the oxide product may be dried and calcined in an inert atmosphere.

Cryochemically processed powders have also been reported, and this method consists of freezing a water solution of the desired materials, followed by sublimation of the ice to leave an intimately dispersed and uniform material. The precipitates are subsequently calcined and ball-milled. Hence, Al_2O_3–MgO powder mixtures have been prepared from Al and Mg sulphates [14].

Oxide ceramic powders may also be prepared by a process of "liquid-drying", consisting of dehydration of an aqueous salt solution in a hygroscopic liquid, accomplished by spraying or atomizing the solution into a vortex of the hygroscopic liquid. The liquid rapidly removes water from the solution droplets, while the remaining metal salt precipitates to form a dry but hygroscopic powder which is subsequently calcined to yield the oxide. The process has been employed for the production of high-purity Al_2O_3 and Fe–Mg–Mn complex oxides [15], and may be applicable to other materials.

Although compaction of the powder prior to sintering may be carried out conventionally (i.e. uniaxially) isostatic pressing is more suitable, as this results in a more uniform distribution of internal stresses and may lead to a more homogeneous sintered product.

3.1.2.2. Solid-state techniques: hot-pressing. Hot-pressing, which involves simultaneously pressing and heating a powder mass, is a widespread technique employed for the production of many optical polycrystalline ceramics. Densification is achieved far more rapidly than in conventional sintering, and problems associated with compact warpage, which may occur during sintering due to local inhomogeneities, are eliminated. However, major technical difficulties are involved including die-compact compatibility, adequate temperature control, and ultra-pure powders must again be employed in order to minimize grain-boundary impurities.

The technique of liquid-phase hot-pressing or sintering is also feasible when one of the components, or an additive, or a eutectic composition, has a lower melting point than the temperature employed. This process may, with relative ease, yield materials approaching the theoretical density, but often results in the formation of grain-boundary films or aggregates.

3.1.2.3. Vapour-phase techniques. Vapour-growth techniques similar to those employed in the preparation of single crystals may be used to prepare high-purity polycrystalline materials and this is discussed more fully in Section 3.2.1, with reference to specific materials.

3.2. Materials reported in the literature

3.2.1. Materials preparation, infra-red transmission, and general properties

3.2.1.1. Single crystals: oxides. Single crystals for optical studies have been grown by a variety of techniques, although, in general, their size has been limited to less than about 50 mm diameter.

For instance, transparent simple oxides including cubic MgO [16, 17], Y_2O_3 and Yb_2O_3 [18], and hexagonal Al_2O_3 [19], and complex oxides including $(Y, La)_2O_3$ [18], $CaWO_4$, $PbWO_4$, $PbMoO_4$ and $Bi_4Ti_3O_{12}$ [20], $Pb_3MgNb_2O_9$ [21], $LiGaO_2$ [22], $LiNbO_3$ [23], together with various spinels and garnets [24–26], have been prepared by Czochralski growth, flux growth or CVD techniques. Transmission of MgO extends to about 9 μm, the Group III and rare-earth oxides to about 7 to 8 μm, and the complex oxides to about 6 μm.

3.2.1.2. Single crystals: non-oxides. Similarly, non-oxide single crystals have been grown, and their size has also been limited, with the exception of certain halides which have been grown to at least 400 mm diameter.

For instance, rhombic sulphur has been reported to transmit well in the 0.8 to 32 μm range, with the exception of bands at 11.8 and 21.6 μm [27], and hexagonal LaF_3 transmit to about 10 μm [28]. $KNiF_3$ and $KMgF_3$ perovskites have been found to transmit to about 9 μm [29], whilst various semiconducting compounds have also been prepared, but their short wavelength transmission is usually limited and they may be opaque to the visible and near infra-red [30]. Other materials including

AlN and BN, prepared as very small single crystals, exhibit good optical quality [31, 32].

3.2.1.3. Polycrystalline materials: sintered oxides. Various optically transparent polycrystalline oxides have been prepared successfully by sintering very pure powders to near theoretical density.

For instance, Mazdiyani *et al.* [33] prepared cubic phase-stabilized ZrO_2 (a minimum of 6% Y_2O_3 being necessary for complete stabilization) from mixed oxides obtained by the alkoxide process. The product was dried and calcined, cold-pressed, and sintered in air to yield a translucent material which transmitted $>50\%$ to beyond $12\,\mu m$.

Transparent Y_2O_3 has been prepared employing ThO_2 as a grain-growth inhibitor. Hence, Jorgensen *et al.* [34] sintered mixed powders prepared by adding thorium nitrate to a Y_2O_3 water-slurry, and similarly, Greskovich *et al.* [35] utilized mixed powders prepared by the sulphate and oxalate processes.

Liquid-phase sintering has also been successfully employed to produce near theoretically dense material in a limited number of systems. For instance, Bratton [36] prepared translucent $MgAl_2O_4$ spinel by employing CaO to induce liquid-phase sintering. The powders were produced by a co-precipitation technique and compacts were vacuum-sintered. Similarly, transparent ferroelectric barium and strontium-doped lead zirconate titanate ceramics have been prepared by Miyauchi *et al.* [37] by employing excess PbO to induce a liquid-phase during sintering.

Finally, transparent materials have also been successfully prepared from certain non-cubic materials. For instance, Kim *et al.* [14] utilized cryochemically prepared Al_2O_3 powders containing MgO as a sintering aid to produce near theoretically dense translucent material; optimum density was obtained with 0.1 to 0.3 wt % MgO.

3.2.1.4. Polycrystalline materials: hot-pressed oxides. Hot-pressing is a more widely employed technique for materials preparation due to the greater ease with which theoretical density can be achieved.

For instance, Dutta *et al.* [38] prepared transparent Y_2O_3 ($>99.6\%$ TD), without additives, by vacuum hot-pressing. Transparent Y_2O_3 has also been prepared by Lefever *et al.* [39] by an extremely laborious technique. Y_2O_3 powder with LiF additive was vacuum hot-pressed in a thin-walled mullite die, and the temperature and pressure were increased until failure of the die occurred and a "forging" action began. Subsequently, the temperature and pressure were further increased and held for 48 h to produce transparent discs ~ 10 mm diameter which transmitted to about $8\,\mu m$.

Other simple oxides, including those of certain rare earths have also been prepared as transparent discs. Hence, Gazza [40] prepared Sc_2O_3, with good transmission to $\sim 6.5\,\mu m$, by incremental heating of the powder under a pressure of $46\,MN\,m^{-2}$ in vacuum, but if the temperature exceeded $1575^\circ C$ cracking of the samples occurred during cooling. Similarly, transparent discs 50.8 mm diameter of Gd_2O_3 were prepared by Carnall *et al.* [41] by vacuum hot-pressing powders prepared by thermal decomposition of a precipitate of gadolinium oxalate with a LiCl densification agent. The material exhibited good transparency to $>6\,\mu m$, although many fine absorption bands were observed attributed to OH^-, HCO_3^- and CO_2^{3-}. The alkaline earth oxide CaO has also been prepared by Gupta *et al.* [42] by vacuum hot-pressing the powder with 0.1 to 1.0 wt % CaF_2. Good transmission in the range 0.5 to $10.0\,\mu m$ was reported, but neither the mechanical properties nor the hygroscopicity were evaluated [43]. However, an earlier investigation by Rice [44] of translucent CaO indicated that transmission may be seriously affected by hydration of the surface of the material.

Finally, Carnall [45] prepared MgO using LiF additive and it was suggested that densification occurs by a process of solution and re-precipitation of MgO in liquid LiF. Other materials prepared by similar techniques also presumably exhibit comparable liquid-phase sintering.

Several complex oxides have been prepared. For instance, Gazza [46] fabricated transparent $LiAl_5O_8$ from powders synthesized from cryo-precipitates and freeze-drying of Li_2CO_3 and $Al(NO_3)_2\,9H_2O$. The calcined compacted powders were vacuum hot-pressed to yield material approaching 100% transparency out to about $5\,\mu m$. Haertling [47] prepared highly transparent ferroelectric ceramics in the lead zirconate titanate system by hot pressing high-purity powders. Haertling *et al.* [48] also prepared (Pb, La)

$(Zr, Ti)O_3$ solid solutions (PLZT) exhibiting good transmission in the 0.4 to 6.0 μm region, from mixed oxides.

Transparent electro-optic ceramics of type (Pb, La) $(Hf, Ti)O_3$ have been prepared by Ainger *et al.* [49] from a blend of Pb, La, Hf and Ti oxides, to yield materials highly transparent in the 0.6 to 7.0 μm range.

The dependence of transmission on grain-size, or on lattice distortion caused by direct substitution of different size atoms within the lattice has also received some attention in the case of ferroelectric ceramics. Hence, Matsuyama *et al.* [50] prepared transparent and theoretically dense PLZT materials of grain sizes in the range 3 to 11 μm from mixed oxides, and noted that transmission in the visible was independent of grain size for the antiferroelectric phase, but decreased with increasing grain size for the ferroelectric phase. The effect of lattice distortion produced by altering the Zr:Ti ratio was studied by Miyauchi *et al.* [51] who observed that transmission increased almost linearly with decreasing lattice distortion.

Finally, as with sintered products, certain transparent non-cubic materials have been prepared. For instance, Dutta *et al.* [52] fabricated translucent hexagonal ZnO by vacuum hot-pressing, and similarly hexagonal BeO has been prepared by Kodaira *et al.* [53] with transmission to $\sim 4.5\,\mu$m. And finally, transparent alumina containing 63% of very finely distributed porosity has been prepared by Yoldas [54] from active, high surface area alumina obtained from alkoxides.

3.2.1.5. Polycrystalline materials: hot-pressed non-oxides. Tetragonal MgF_2 was prepared by Smyth *et al.* [55] by hot-pressing in air, but the material was transparent only if the pressure was applied after the powder had attained the hot-pressing temperature. More recently an extensive investigation of hot-pressed MgF_2, ZnS, ZnSe and MgO prepared as discs, or as pre-fabricated domes up to 216 mm diameter, was reported by Latimer *et al.* [56]. In all instances, very pure powders were necessary to produce good visible and near infra-red transparency. MgF_2 could be hot-pressed in air, but vacuum was required for the other materials. Finally, hot-pressed CdTe, opaque to the visible, but exhibiting useful transmission in the 1 to 30 μm range, has been prepared by Ladd [57]; however, the mechanical properties of this material are inadequate for the majority of applications.

3.2.1.6. Polycrystalline materials: materials prepared by CVD. This technique has been very successfully employed for the preparation of polycrystalline ZnS and Zn (S, Se) in the form of plates 254 mm x 254 mm x 15.9 mm in size, and also as hemispherical domes 229 mm in diameter [58]. Optimum conditions for deposition of ZnS were 650° C in the presence of excess Zn vapour, and the material was transparent in the 0.5 to 13.5 μm range. These materials were also harder and of better optical quality than similar materials produced by more conventional techniques, although scattering losses were apparent, which were attributed to the co-existence of both hexagonal and cubic forms of ZnS in the final product.

Crystalline and amorphous forms of Si_3N_4 up to 4.6 mm thick have been prepared by Niihara *et al.* [59] also using the CVD technique, using a mixture of $SiCl_4$, NH_3 and H_2, for a deposition temperature in the range 1100 to 1500° C at a total gas pressure of 5 to 300 Torr. Thin sections were transparent to the visible, but became opaque as the thickness was increased.

3.2.2. Effect of temperature on infra-red transmission

The effect of low temperatures, down to −180° C, on the infra-red transmission of strontium titanate has been studied by Salzberg [60] who noted very little dependence. However, the useful transmission limit of sapphire, investigated by Oppenheim *et al.* [61], fell to about 4 to 4.5 μm at 1000° C compared to 5.0 μm at 20° C. Similarly, Gryunak *et al.* [62] also reported a slight increase in the absorption coefficient of sapphire with temperature up to 2020° C.

Transmission of single crystals of MgO and BaF_2 in the temperature range 27 to 1000° C has also been studied by Oppenheim *et al.* [63]. The useful transmittance of MgO was reduced from a long wavelength limit of about 8.0 μm at 27° C to about 6.0 μm at 1000° C, whilst that of BaF_2 was reduced from 12 to 13 μm to about 8 μm.

Finally, the transmittance of various materials including fused quartz, calcium aluminate glasses, single crystals of sapphire, NaCl, AgCl, Si and Ge, and polycrystals of MgF_2 and ZnS has been

investigated in the range 25 to 400° C by Gillespie *et al.* [64]. Only a slight decrease in transmission was observed for the dielectric materials, whilst significant shifts were noted in the long-wavelength limit of the semiconductors, with Ge exhibiting zero transmission at 400° C.

3.2.3. Mechanical properties and methods of strengthening materials

3.2.3.1. Strength and toughness. The strengths, together with other properties, of infra-red transmitting ceramics are summarized in Table II. Only quite recently have serious attempts been made to investigate the fracture mechanisms operative with specific infra-red materials.

For instance, Evans *et al.* [65] carried out a fracture mechanics study of ZnSe suitable for laser window applications, and concluded that fracture is controlled primarily by the presence of surface flaws. CVD ZnSe exhibits low strength and fracture toughness, typical values being of the order of $50\,MN\,m^{-2}$ for MOR in 4-point bend, and $0.9\,MN\,m^{-3/2}$ for K_{IC}. Slow crack growth under static fatigue conditions could be detected consistently by an acoustic emission technique, and preliminary work suggested that the lifetime requirements of laser windows can be achieved by overload proof testing to a proof ratio of 1.35.

Crack propagation studies have also been carried out on CVD ZnTe by Feimen *et al.* [66] using a double cantilever beam technique. It was noted that the rate of crack propagation as a function of K_{IC} was larger when samples were tested in humid conditions. MOR in 3-point bend was also found to decrease from $40\,MN\,m^{-2}$ to $29\,MN\,m^{-2}$, and failure resulted from flaws contained in one or two larger grains.

3.2.3.2. Rain-erosion resistance. A number of investigations have been reported in which various materials have been subjected to conditions simulating rain-erosion, but much of the data are not freely available. Rainfall conditions can be simulated by a spinning-disc technique, or alternatively a "rocket-sled" may be employed to simulate high-velocity conditions [67].

Coenen *et al.* [68] noted that a general trend of increasing rain-erosion resistance for material of increasing E was generally observed, although the scatter in the results was quite large.

The erosion-resistance of reaction-sintered Si_3N_4 has been reported by Walton [67] for simulated rainfall at $25.4\,mm\,h^{-1}$ and $223\,m\,sec^{-1}$ using 6.4 mm thick samples, to be moderate to severe in 360 to 480 min depending on whether the surface was ground or unground. Walton also concluded that caution should be employed when attempting to predict the expected behaviour of a given material by extrapolation from one velocity to another. Hence, slip-cast silica evaluated at a velocity of Mach 3 showed no erosion damage when in the surface glazed condition, but slight erosion when unglazed, whilst at Mach 5, damage to the glazed material was greater than that to the unglazed material.

3.2.3.3. Methods of strengthening materials: bulk methods. Chin *et al.* [69] observed that stengthening of single crystal alkali halides by divalent-ion additions, Ca^{2+}, Sr^{2+} or Ba^{2+}, was dependent only upon the concentration of dopant and was independent of the species. Presumably, this apparent independence can be expained on the basis of similar ionic sizes.

The creep behaviour of doped and un-doped single LiF crystals in the temperature range 650 to 750° C was investigated by Ruoff *et al.* [70], and found to be similar to that of pure metals. A lower creep rate was obtained for the Mg-doped samples and a model was proposed based on dopant cation vacancy complexes and binding of dopant to charged dislocations.

Buch *et al.* [71] investigated the compressive yield strength of polycrystalline CdTe as a function of grain size in the range 6 to 10 μm, and observed that the 0.5% offset yield strength in compression increased linearly proportional to $d^{-1/2}$, from 50 to $65\,MN\,m^{-2}$.

A fibre-reinforced material has been produced by directional solidification of a NaF–NaCl eutectic which yielded aligned rods in a NaCl-rich matrix [72]. Although mechanical strength was not evaluated it would be expected that such a material would be significantly tougher and possibly stronger than the homogeneous matrix. Unfortunately, infra-red transmission was severely reduced in the near infra-red, although this is not surprising in view of the significant difference in the refractive indices of the two phases.

Reference to metal fibre-reinforced ceramics for possible radome applications has been made by

TABLE II Properties of selected crystalline materials

Material	Reduced mass (atomic units)	Lattice parameter (10^{-10} m)	C_{11} (GN m^{-2})	E (GN m^{-2})	Knoop hardness (kg mm^{-2})	MOR (MN m^{-2})	T_m (° C)	α (10^{-6} ° C^{-1})	Refractive index		Water solubility (g per 100 g water at 20° C)	Density (g cm^{-3})
									At 1 μm	At 4 μm		
LiF	5.08	4.027	112	64.8–88	108	–	870	37 (0–100° C)	1.387	1.349	0.27	2.635
NaF	10.40	4.628	97.1	80.3	–	–	980	36 (20° C)	1.322	1.308	4.2	2.558
RbF	15.54	5.640	55.2–57	–	–	–	795	–			130.6	3.557
MgF_2	10.66	3.060	177–204	–	576	150	1255	11 (25–200° C)	1.378	1.353	0.76×10^{-2}	–
CaF_2	12.89	5.462	165	80–140.8	158	37	–	20 (25–200° C)	1.429	1.410	0.13×10^{-2}	3.180
BaF_2	16.69	6.200	90.4	53.1–65	82	–	1280	18.4 (0–300° C)	1.468	–	0.12	4.89
NaCl	13.95	5.650	48.5	40–43.7	16.7	3.9	801	44 (–50–200° C)	1.532	1.522	36	2.165
KCl	18.59	6.291	39.8	29.7–38.2	7.7	4.4	776	36 (20–60° C)	1.478	–	34.7	1.984
RbCl	25.06	6.548	36.5	–	–	–	718	–	1.493 (0.590 μm)		77 (0° C)	2.80
$BaCl_2$	28.18	9.421	–	–	–	–	963	–	1.742 (0.590 μm)		37.5	3.856
CuCl	22.76	5.406	–	–	–	–	422–430	–	–		0.62×10^{-2}	4.14
AgCl	26.68	5.556	59.4–60.1	20–32.9	9.5	–	458	30 (20–60° C)	2.022	2.000	0.15×10^{-3}	–
$PbCl_2$	30.27	4.535	40.6	–	–	–	501	–	–	–	0.99	5.85
KBr	26.25	6.580	34.5	26.9–33	6.5	3.3	730	43 (20–60° C)	1.544	1.535	65.2	2.75
CsBr	49.90	4.296	30.0	26.7	19.5	–	636	48 (20–50° C)	1.678	1.668	124.0	–
$CaBr_2$	26.69	4.342	–	–	–	–	730	–	–	–	142.0	3.353
$SrBr_2$	41.79	7.155	–	–	–	–	643	–	1.575 (0.590 μm)		100.0	4.216
$BaBr_2$	50.52	9.919	–	–	–	–	850	–	1.75 (0.590 μm)		104.1	4.781
CuBr	35.40	5.691	–	–	–	–	498	–	–	–	–	4.77
NaI	19.46	–	30.4	–	–	–	661	–	1.775 (0.590 μm)		185.0	3.667
KI	29.89	7.070	27.1	26–31.5	–	–	681	42.6 (40° C)	1.640	1.627	144.0	3.13
RbI	51.07	7.347	25.6–25.9	–	–	–	647	–	1.647 (0.590 μm)		152.0	3.55
CsI	64.92	4.567	24.6	22	–	–	621	50 (25–50° C)	1.757	1.743	85.5	4.510
BaI_2	65.96	10.695	–	–	–	–	740	–	–	–	170 (0° C)	5.15

ZnS	21.51	5.423	94.2–107.9	50	178	97	1020 (trans)	6.9 (25–200° C)	2.301	–	0.69×10^{-4}	4.102
CdS	24.95	5.582	81–84.3	46	97	–	1727	6.5 (40–200° C)	2.341	–	0.13×10^{-3}	–
PbS	27.77	5.935	127	116	–	–	1114	19.4 (40–200° C)	4.1 (3.0 μm)		0.86×10^{-4}	7.5
ZnSe	35.76	5.668	81.0	–	–	41	1517	7.4 (25–200° C)	2.89 (0.590 μm)		insoluble	5.42
ZnTe	43.22	6.101	71.3	–	–	–	1237	–	3.56 (0.590 μm)		–	6.34
CdTe	59.76	6.477	53.5–61.5	23	54	32	1041	5.3 (27° C)	–	–	insoluble	6.20
SiC	8.41	4.348	560	405	2880	–	2797	5.12 (25–1000° C)	–	–	insoluble	3.217
C (diamond)	6.01	3.567	949	908	8820	–	> 3550	~ 2.0	2.417 (0.590 μm)		insoluble	3.51
Si	14.04	5.420	167	134.5	1240	–	1420	~ 3.1 (100–200° C)	–	3.426	insoluble	2.32–2.34
Ge	36.30	5.646	129	102.7	959	–	937	~ 6.2 (25° C)	–	4.022	insoluble	5.35
BeO	5.77	4.39	–	295–314	–	–	2550	9.03 (25–1000° C)	–	1.733	0.2×10^{-4}	3.01
MgO	9.60	4.213	290	248.9	692	138	2800	13.8 (20–1000° C)	1.723	1.631	0.62×10^{-3}	3.58
CaO	10.43	–	200	–	–	–	2600	–	1.838 (5.138 μm)		0.131	3.25–3.38
Se_2O_3	11.80	9.810	–	245.9	910	218	–	–			insoluble	3.864
Y_2O_3	13.56	10.604	–	–	760	–	2410	–	–	–	0.18×10^{-3}	5.01
Yb_2O_3	14.65	–	–	–	–	–	–	–	–	–	insoluble	9.17
TiO_2	12.00	–	358–484	351	879	–	–	8.12	2.483	2.350	insoluble	4.26
Ga_2O_3	14.52	–	–	–	670	–	–	–	1.962 (0.590 μm)		–	7.55
Al_2O_3	10.05	12.97	563	460.8	1370	450	2030	8.52 (25–1000° C)	1.755	1.664	0.98×10^{-4}	3.97
SiO_2 (quartz)	10.18	5.394	116.6	101	741	–	1610	10.67	1.535	1.466	insoluble	2.635–2.66
GeO_2 hex.	13.15	5.64	–	–	–	–	1115	–	–	–	0.447	4.228
tet.		2.866	–	–	–	–	1086	–	–	–	insoluble	6.239
$MgAl_2O_4$	9.60	8.083	279–300.5	–	1140	–	2050–2135	5.9 (40° C)	1.727 (0.590 μm)		–	3.6
$SrTiO_3$	12.00	3.905	315.6	265	595	–	2080	–	2.315	2.168	–	–
$BaTiO_3$	12.00	4.038	283	93	–	–	1600	–	2.40 (0.590 μm)		–	6.017
$CaWO_4$	10.43	11.372	–	–	390	–	1535	–	1.918 (0.590 μm)		0.64×10^{-3}	6.062
$LiAl_5O_8$	4.84	7.909	–	386	1925	207–241	–	–	–	–	–	–

Krochmal [73] who reviewed the "state-of-the-art", although the extent to which metal fibre additions can be tolerated at radar frequencies was not established, and such materials would not be suitable for use at infra-red frequencies.

3.2.3.4. Methods of strengthening materials: surface methods. Kirchner [74] reported the strengthening of polycrystalline alumina, spinel, titania and zirconia, and single crystal sapphire by quenching or glazing. Quenching imposes a size limitation but is quite successful in improving flexural and tensile strength, thermal-shock and impact resistance, and delayed fracture performance.

An investigation to determine whether or not quenched alumina retains its improved strength at elevated temperatures, when stress relief mechanisms are expected to be operative, has also been carried out by Kirchner *et al.* [75]. The results exhibited a considerable degree of scatter, although strength retention was observed up to about 1000° C and impact energy was similarly improved.

The strengthening of hot-pressed Si_3N_4 by heating and quenching has also been reported by Kirchner *et al.* [76]. It was noted that quenching from temperatures > 1400° C did not increase the strength whereas quenching from 1350 to 1400° C did. The effect of the rate of quench was also studied, and it was found that slow cooling, when residual compressive surface stresses would not be expected to be present, also increased the strength to a similar degree as quenching. The strength of cylindrical rods could be increased from about 700 MN m^{-2} to about 950 to 1000 MN m^{-2}, although a large degree of scatter is apparent in the results.

Physical alteration of a materials surface has also been employed to improve strength. Hence, Doherty *et al.* [77] strengthened sapphire rods by application of lower expansion materials at high temperatures. A calcium aluminate coating could be applied by packing a sapphire rod in $CaCO_3$ and heating at 1350° C for 3 h.

Surface coatings may also be employed as anti-reflection aids to minimize high reflection losses associated with materials of high refractive index. The criteria for an anti-reflection coating are: (a) the refractive index of the coating, n', equals the square root of the substrate refractive index ($n' = (n)^{1/2}$), (b) the phase difference between the incident wave and the reflected wave is an odd multiple of π; ($nd \cos\theta = (\lambda/4)(2m + 1)$, where d = film thickenss, and θ = angle of inclination in the film of the ray to the film normal, and m is an integer). Hence, it is apparent that there is an optimum film thickness for a given wavelength, and a coating is not fully effective throughout the entire spectrum. Consequently, a film thickness equal to $\lambda/4$ at the position where peak transmittance is desired is usually employed.

The coating may be applied by vacuum deposition, or thermal treatment may be employed for some materials including Si [78]. More recently multi-layer coatings have been utilized for improving transmittance of selected materials over a wide wavelength range. For instance, Church *et al.* [79] employed Si + ThBr + PbF + SiF coatings on Ge.

A disadvantage of coated materials is that in a situation where the coating is eroded, transmittance will be correspondingly reduced, and as the coatings are usually very thin (typically ~ 1 μm) they are not ideal for adverse service conditions, such as rain-erosion. However, if the refractive indices of coating and substrate are matched it may be feasible to coat selected materials with relatively thick layers of abrasion-resistant materials by plasma-spraying, r.f. sputtering or CVD techniques, although little work has been reported on this.

4. Relationships between mechanical and physical properties and infra-red transmission

An attempt has been made to establish simple relationships between the mechanical and physical properties and the infra-red transmission of various materials for which data are available, from which the feasibility of improving the infra-red transmission and/or the properties of existing materials or of establishing possible new materials or areas for research may be evaluated.

Figure nomenclature

A. Crystalline materials

1	LiF	9	CaCl
2	NaF	10	AgCl
3	MgF_2†	11	TlCl
4	CaF_2†	12	KBr
5	BaF_2	13	CsBr
6	NaCl	14	CuBr
7	KCl	15	TlBr
8	RbCl	16	KI

17	RbI	33	$BaTiO_3$
18	CsI	34	$PbMoO_4$
19	BeO*	35	$LiAl_5O_8$
20	MgO†	36	Diamond
21	CaO†	37	Si†
22	Sc_2O_3*	38	Ge†
23	Y_2O_3*	39	Te
24	Gd_2O_3*	40	ZnS*
25	TiO_2	41	CdS
26	Al_2O_3	42	ZnSe*
27	Al_2O_3 ("Lucalox")*	43	CdTe*
28	Y_2O_3–ThO_2 ("Yttralox")*	44	GaAs
29	Mullite*	45	GaSb
30	$MgAl_2O_4$†	46	InSb
31	$CaWO_4$	47	NbC*
32	$SrTiO_3$	48	SiC†

*Polycrystalline. †Polycrystalline and single crystal samples reported. All others are single crystal.

B. Glasses

a	SiO_2	h	IRG3 (dense flint)
b	GeO_2	i	IRG7 (lead silicate)
c	Se	j	IRG9 (fluorophosphate)
d	BS37A (calcium aluminate)	k	9754 (germanate)
e	BS39B (calcium aluminate)	l	Al_2O_3–BaO–CaO
f	Tellurite	m	Silicate glass-ceramic
g	As_2S_3	n	Magnesium alumino-silicate glass-ceramic

4.1. Prediction of infra-red transmission using the simple diatomic oscillator model

Substituting $C_{11}x$ for f, the force constant, into Equation 9, the wavenumber of the fundamental absorption, ν_f, may be given by:

$$\nu_f = \frac{1}{2\pi c}\left(\frac{C_{11}x}{\mu}\right)^{1/2} \qquad (13)$$

where c is the velocity of light.

For c, C_{11} and x in SI units, and μ in atomic units,

$$\nu_f = 130\left(\frac{C_{11}x}{\mu}\right)^{1/2} \text{ cm}^{-1} \qquad (14)$$

and

$$\nu_f = 10^4/\nu_f\,\mu\text{m}.$$

For non-cubic materials C_{33} may be substituted in place of C_{11} if $C_{33} > C_{11}$, and similarly z may be substituted for x (in general, the highest value of $C_{xy}a$ should be employed).

The first overtone often sets the useful transmission limit, and this may be taken as approximately equal to half the fundamental wavelength (although this is an over-simplification since the actual positions of overtones are dependent on the anharmonicity of the vibration). More accurate predictions of the fundamental require a detailed knowledge of the shape and size of the lattice, together with the values of force constants, and this information is only available for a limited number of materials. However, if a significant trend can be established by employing a simple relationship for which data are readily available, a qualitative estimate of the infra-red capability of new or candidate materials should be feasible, and this is the primary aim of this assessment. Before considering this aspect in greater detail, the effect of the type of material and of the sample thickness is first summarized.

A characteristic transmission versus wavelength curve of the type illustrated in Fig. 1 is obtained for many materials, particularly those which exhibit a highly ionic bonding component. Superimposed onto this basic curve may be other absorption bands and fine structure, depending on sample thickness, instrument sensitivity, and the effect of second-order absorptions. The important quantities are the cut-on and cut-off wavelengths, and also the corresponding values for 50% transmission which is taken here as the minimum useful transmission. These values are dependent on the refractive index of the material, which determines the amount of radiation reflected from the external surfaces, and on the absorption coefficient of the material, and hence on the sample thickness. If the sample thickness is increased, the values of the cut-on and cut-off wavelengths tend to converge thereby limiting the useful transmission range. The variation of 50% cut-off with sample thickness is illustrated in Fig. 2 for a variety of materials, and, in general,

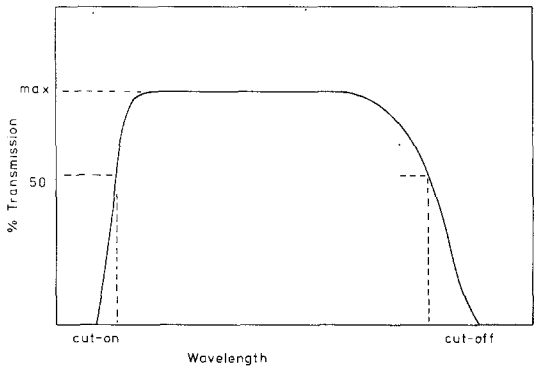

Figure 1 Typical transmission versus wavelength curve of a hypothetical polar material.

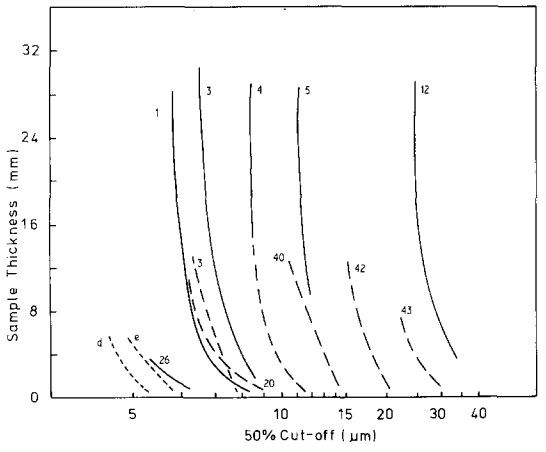

Figure 2 Variation of 50% infra-red cut-off with sample thickness for a variety of materials. Full line – polycrystalline; broken line – single crystal; dotted line – glass.

the rate of change of transmission with sample thickness is greatest at small thicknesses.

As previously outlined, the total cut-off value is generally dependent on first-order absorption, and for highly ionic materials in particular, it may often be set by the position of the first overtone. The value of the total cut-off can usually only be approximated since accurate measurement is difficult due to limitations in instrument sensitivity etc., and most transmission curves reported in the literature do not give the total cut-off value, and hence extrapolation of data is necessary.

The values of the total cut-off are plotted against the approximated theoretical value of the first overtone in Fig. 3 for a variety of materials for which data are available. The experimental transmissions are shown within the limits set by the thicknesses of the samples that have been studied, rather than by attempting to extrapolate further to a standard thickness. The data are also summarized in Table III.

It is evident that, in general, the predictions are fairly accurate, particularly when considering the gross approximations that have been employed in their determination. For instance, taking the experimental value of cut-off for the thinnest samples studied (generally ~ 1 to 3 mm) the ratio of theoretical to experimental strength falls in the range 1.06 to 1.16 for single crystal MgO, NaF, CaF_2, NaCl, KCl, CsI, $BaTiO_3$, and polycrystalline $MgAl_2O_4$ (0.37 mm thick); 1.16 to 1.39 for single crystal LiF, CsBr, and $MgAl_2O_4$ (5.45 mm thick) and polycrystalline MgO and CdTe; 1.39 to 1.65 for single crystal BaF_2, and polycrystalline ZnS and ZnSe; 1.65 to 1.82 for single crystal MgF_2 and TiO_2, and >1.82 for SiO_2 and polycrystalline MgF_2. The ratio is less than unity for single crystal AgCl (0.87), KBr (0.94), KI (0.87), and Al_2O_3 (0.56).

Highly covalent materials generally absorb due to second-order effects, and hence do not exhibit a characteristic absorption curve similar to that shown in Fig. 1. These materials often exhibit a series of fairly well-resolved absorption bands, and the overall transmission may extend out to long wavelengths. If these materials are considered on the arbitrary basis to taking the first absorption band for which transmission falls to a value of $<10\%$, for useful thicknesses, as due to first overtone absorption by an induced dipolar oscillation, and calculating the expected absorption band on this basis, the agreement for diamond, Si, Ge, and SiC is remarkably accurate. Hence,

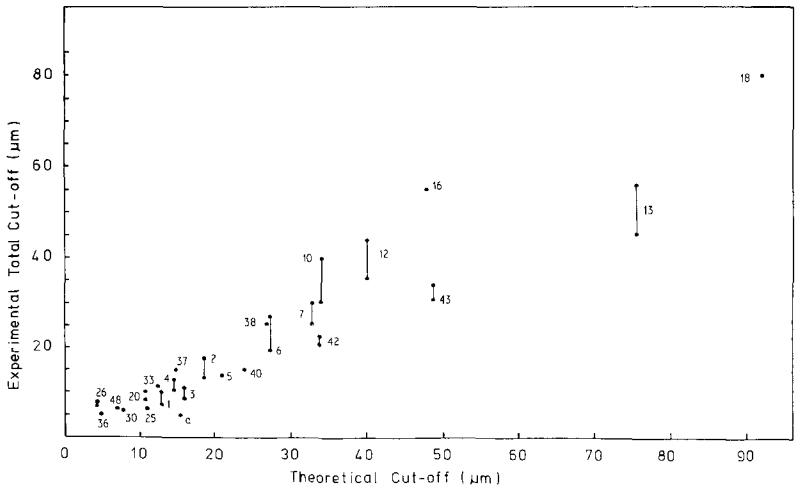

Figure 3 Experimental total infra-red cut-off versus theoretically derived total cut-off values for a variety of materials.

TABLE III Experimental transmission data compared to the theoretical first overtone absorption bands, assuming the simple diatomic oscillator model

Material	Transmission data			Theoretical cut-off (μm)
	Experimental			
	Sample thickness (mm)	Total cut-off (μm)	50% cut-off (μm)	
LiF	1–27	7.0–10.0	5.8–8.0	12.9
NaF	1–10	13.0–17.5	10.3–13.9	18.5
MgF_2	2–30	8.0–11.0	6.5–8.5	15.9–17.1
MgF_2*	2–12	7.6–8.0	6.4–7.6	15.9–17.1
CaF_2	3–33	10.0–12.5	8.5–10.0	14.6
CaF_2*	2–12	10.9–12.7	8.7–10.4	14.6
SrF_2	3–27	12.0–13.5	9.8–12.4	–
BaF_2	9–27	13.0–14.0	11.0–12.0	21.0
LaF_3	0.5	–	10.0	–
CdF_2	5	13.0	10.4	–
NaCl	1–26	19.0–27.0	15.2–21.5	27.4
KCl	5.3–27	25.0–30.0	19.0–22.5	33.1
RbCl	3.0	–	~ 30	39.4
CuCl	3.92	–	19.0	–
AgCl	1.1–10.0	30–40	23.5–27	34.5
KBr	4–27	35–44	25–33	41.4
CsBr	5.1–25	45–56	40–44	75.7
CuBr	2.92	33	26	–
KI	0.83	55	41	48.0
RbI	3.91	–	~ 50	62.9
CsI	3–5	~ 80	56–60	92.3
ZnS*	2–12	14.6–15.2	10.7–13.8	23.3–25
CdS*	3.9	–	14.4	28.0–28.6
PbS	–	–	–	23.3
ZnSe*	2–12	20.2–22.4	15.3–19.6	33.9
ZnTe	–	–	–	28.3
CdTe*	2–6	30.2–34	23.2–27.6	47.1–50.5
SiC	0.27	6.0–6.5	5.0	7.2
Si_3N_4	0.66	4.6	–	–
C (diamond)	1.88	5.0 first absorption		5.1
Si	0.5	~ 15 band, < 10%		15.1
Ge	–	~ 25 transmission.		27.1
BeO*	0.8	–	4.5	–
MgO	0.67	10	9	10.8
MgO*	2–12	7.9	6.3–7.9	10.8
CaO*	1.27	12.6	10.0	–
Sc_2O_3*	2	–	6.5	–
Y_2O_3*	2.5	–	7.0	–
Gd_2O_3	0.5	–	6.5	–
Yb_2O_3*	–	–	8.0	–
TiO_2	2–6	6.0–6.2	4.7–5.4	11.2
Y_2O_3–ZrO_2*	–	–	12.0	–
Al_2O_3	1.0–2.6	7.0–8.0	5.8–6.0	4.5
Al_2O_3*	0.5	8.0	6.6	4.5
SiO_2	10	–	3.5	15.4
SnO_2	–	–	6.5	–
$MgAl_2O_4$	5.45	5.8	5.0	7.7
$MgAl_2O_4$*	0.37	7.5	6.5	7.7
$SrTiO_3$	0.26–10	–	4.5–6.5	12.0
$BaTiO_3$	0.094–0.25	11.2	7.2–7.8	12.5
$CaCO_3$	–	–	3.5	–
$CaWO_4$	2.54	7.0	5.2	–
$PbMoO_4$	3.0	5.9	–	–
$PbWO_4$	2.29	5.6	–	–
$LiAl_5O_8$*	2.5	–	5.5	–

*Polycrystalline materials.

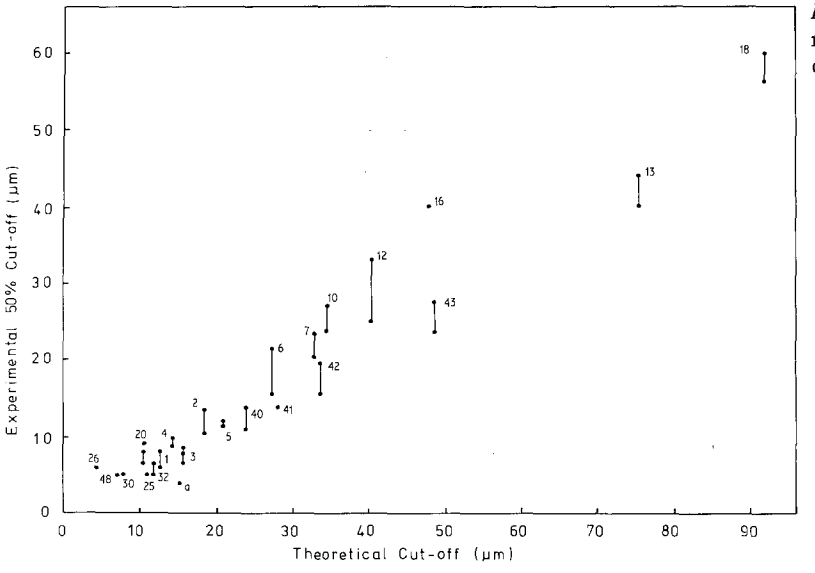

Figure 4 Experimental 50% infrared cut-off versus the theoretically derived total cut-off values.

the ratios of theoretical to experimental values are 1.11 (SiC), 1.08 (Ge), 1.02 (diamond) and 1.01 (Si).

The values of 50% cut-off, which are more accurately known, and which are more important from a practical viewpoint, are also plotted against the expected first overtone values in Fig. 4. In this instance, it is to be expected that the experimental values will be less than the corresponding predicted values since the former have been taken to the short wavelength side of the absorption band. This is true in all the cases cited, with the exception of Al_2O_3.

That the theoretically predicted values are generally too high is not surprising in view of the fact that it has been assumed that C_{11}, or C_{33} in the case of non-cubic materials if $C_{33} > C_{11}$, is much greater than the other elastic constants. The assumption $C_{11}\, a \sim f$ is expected to become less accurate as C_{11} tends towards the values of the other elastic constants, due to the increasing interaction. In general, if the ratio of C_{11} or C_{33} to the next highest elastic constant is small, the predicted transmission is more accurate than when the ratio is high.

In addition the materials for which high inaccuracy of the predicted transmission is obtained, i.e. Al_2O_3, SiO_2 and MgF_2, are also non-cubic. Similarly, the prediction for polycrystalline materials is also generally less accurate than that for single crystals, and the overall interpretation of the discrepancies is hence complicated and likely to be a function of all three factors. The data are summarized in Table IV.

Other parameters may be substituted for C_{11} (or C_{33}) into the fundamental equation. Hence, for cubic materials, if $C_{11} \gg C_{12}$, E may be di-

TABLE IV Inverse ratio of the highest value elastic constant to the second highest, for a selection of materials

Material	Highest value elastic constant ($GN\,m^{-2}$)	Second highest value elastic constant	Ratio
LiF	112	45.6	$C_{12}/C_{11} = 0.407$
NaF	97	24.3	$C_{12}/C_{11} = 0.251$
MgF_2	204	140	$C_{11}/C_{33} = 0.69$
CaF_2	165	47	$C_{12}/C_{11} = 0.285$
BaF_2	90.4	40.6	$C_{12}/C_{11} = 0.449$
NaCl	48.5	12.3	$C_{12}/C_{11} = 0.254$
KCl	39.8	6.2	$C_{12}/C_{11} = 0.156$
AgCl	59.4	36.2	$C_{12}/C_{11} = 0.609$
KBr	34.6	5.6	$C_{12}/C_{11} = 0.162$
CsBr	30.7	8.4	$C_{12}/C_{11} = 0.274$
KI	27.4	4.4	$C_{12}/C_{11} = 0.161$
CsI	24.6	6.7	$C_{12}/C_{11} = 0.272$
SiC	560	500	$C_{11}/C_{33} = 0.893$
MgO	293	92	$C_{12}/C_{11} = 0.314$
CaO	200	61	$C_{12}/C_{11} = 0.305$
TiO_2	484	273	$C_{11}/C_{33} = 0.564$
Al_2O_3	497	495	$C_{11}/C_{33} = 0.996$
SiO_2	116.6	110.4	$C_{33}/C_{11} = 0.947$
ZnS	94.4	56.8	$C_{33}/C_{11} = 0.599$
CdS	81	80	$C_{33}/C_{11} = 0.988$
ZnSe	81	48.8	$C_{33}/C_{11} = 0.602$
CdTe	61.5	43	$C_{33}/C_{11} = 0.699$
C (diamond)	949	151	$C_{12}/C_{11} = 0.159$
Si	167	65	$C_{12}/C_{11} = 0.389$
Ge	129	48.3	$C_{12}/C_{11} = 0.374$
$BaTiO_3$	283	187	$C_{33}/C_{12} = 0.661$
$MgAl_2O_4$	300.5	153.7	$C_{12}/C_{11} = 0.511$

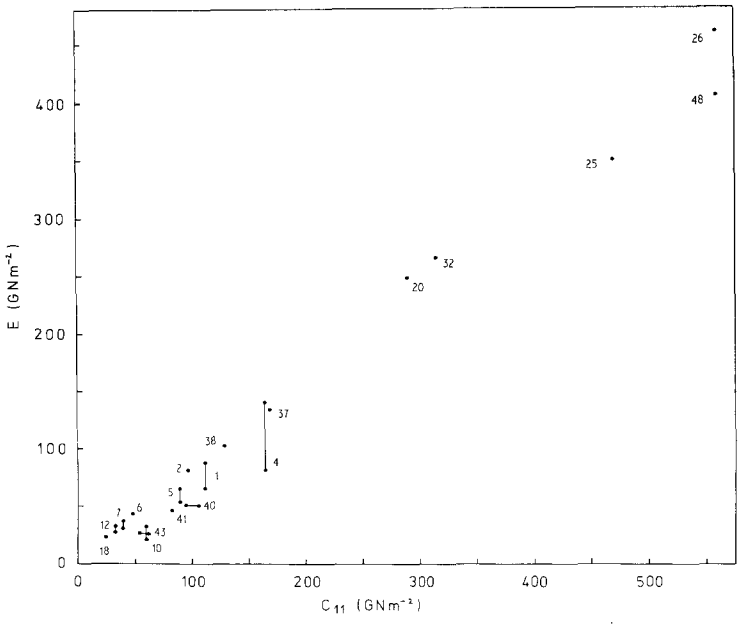

Figure 5 Relationship between the elastic constant C_{11}, and Young's modulus, E, for a variety of materials.

rectly substituted for C_{11}. However, the situation is complicated for polycrystalline materials for which there is no general relationship between the modulii of elasticity and that of the analogous single crystal.

Reference to Fig. 5 indicates that the approximation $C_{11} \sim E$ is not very satisfactory, but the general trend of increasing C_{11} with increasing E is very apparent, and substitution of E for C_{11} into Equation 13 can be made on a qualitative basis to give a good indication of the relative transmission to be expected by a given material (Fig. 6). The values of the parameter,

$$f(E) \propto 1/\left(\frac{Ex}{\mu}\right)^{1/2}$$

have been normalized to give $f(E)$ CsBr = 1.000. It is apparent that there is a critical value of the parameter corresponding to a wavelength of approximately 7.5 μm for values above which transmission improves markedly. This occurs at $f(E) \sim 0.25$ (normalized) for E in GNm^{-2}, x in Å and μ in atomic units.

Similarly, further substitution on a qualitative basis may be made using quantities which are expected to be related to C_{11} or E, including hardness or melting point (T_m). And similarly general trends of increasing transmittance with increasing values of the parameter are found. For hardness, a critical value is again observed, corresponding to a wavelength of $\sim 7.5\,\mu$m at f (knoop hardness) ~ 0.11 (normalized), and for melting point at $\lambda \sim 6\,\mu$m at $f(T_m) \sim 0.25$ (normalized) (Figs. 7 and 8). It should be noted however, that T_m is a reflection of the weakest bonding, and hence some materials of low T_m may still exhibit high-frequency lattice vibrations.

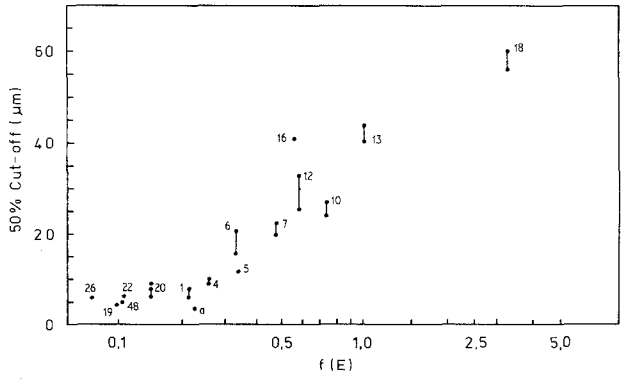

Figure 6 Variation of the 50% infra-red cut-off with $f(E) = 1/(Ex/\mu)^{1/2}$.

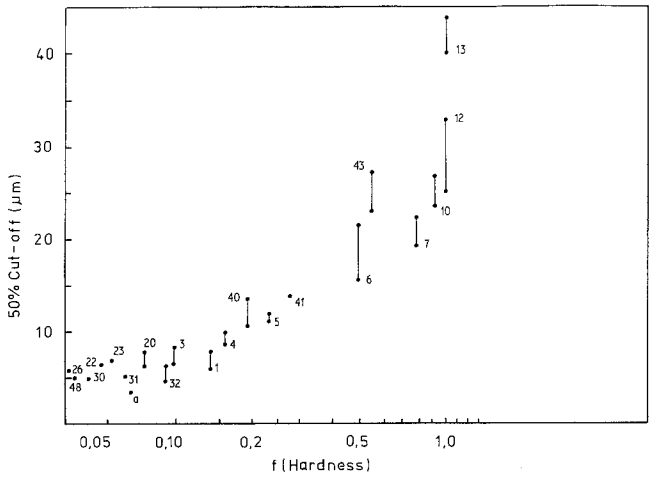

Figure 7 Relationship between 50% infra-red cut-off and f (knoop hardness).

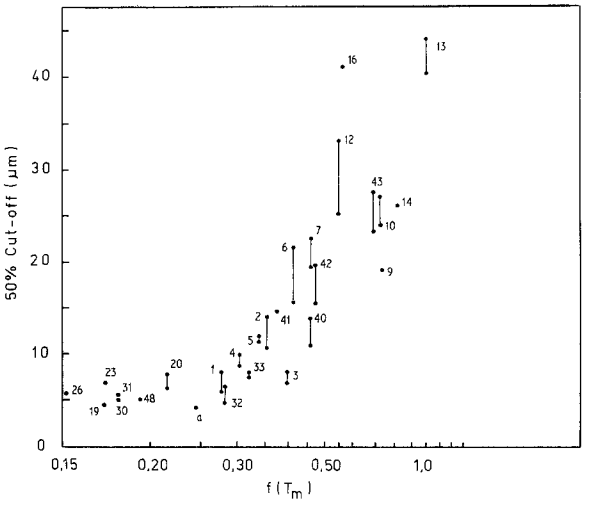

Figure 8 Variation of the 50% infra-red cut-off with $f(T_m)$.

Hence, any material for which values of the parameters are greater than the critical values may be expected to transmit usefully to at least 6.0 to 7.5 μm, assuming that the normal additional conditions are met (i.e. materials are of sufficient purity etc). However, these predictions are only a guide, and materials for which the parameters are less than the critical may still transmit well to about 6 μm, or slightly higher, as shown, for instance, by MgO. Conversely, some materials, including silicon, which also exhibit values near to the critical may display low transmission. Nevertheless, despite these deficiences the parameters should provide useful guide-lines when developing new materials

The correlation breaks down when other quantities are substituted for either C_{11} or $C_{11}x$. Hence, thermal expansion, diatomic bond strength, free energy of formation, and heat of fusion yield no useful correlation.

The normalized values of the parameter:

$$f(X) = 1/\left(\frac{Xx}{\mu}\right)^{1/2},$$

for $X = E$, hardness, melting point, thermal expansion and diatomic bond strength are summarized in Table V.

4.2. Direct relationships between infra-red transmission and mechanical and thermodynamic quantities

4.2.1. Mechanical data

From the simple diatomic oscillator, assuming the force constant is related to C_{11}, E, hardness and also modulus of rupture, a general trend of decreasing transmission with increasing values

TABLE V Values of the parameter $\frac{1}{(Xx/\mu)^{1/2}}$, where $X = E$, α, T_m, hardness or diatomic bond strength, for a variety of materials (normalized to CsBr).

Material	$\frac{1}{(Xx/\mu)^{1/2}}$				
	$X = E$	Hardness	T_m	α	Bond strength
LiF	0.182–0.212	0.140	0.281	0.376	0.277
NaF	0.253	–	0.356	0.508	0.403
RbF	–	–	–	–	0.444
MgF_2	–	0.101	0.393	1.144	0.513
CaF_2	0.195–0.261	0.158	0.311	0.700	0.395
BaF_2	0.309–0.341	0.234	0.341	0.776	0.401
NaCl	0.361–0.376	0.499	0.415	0.482	0.458
KCl	0.421–0.479	0.802	0.459	0.583	0.493
$RbCl_2$	–	–	–	–	0.562
$BaCl_2$	–	–	–	–	0.484
CuCl	–	–	0.741	–	0.646
AgCl	0.579–0.742	0.921	0.756	0.813	0.729
$PbCl_2$	–	–	0.852	–	0.876
KBr	0.527–0.583	1.014	0.548	0.620	0.602
CsBr	1.000	1.000	1.000	1.000	1.000
CuBr	–	–	0.822	–	0.810
TlBr	–	–	–	–	1.228
KI	0.555–0.611	–	0.563	0.640	0.677
RbI	–	–	–	–	0.867
CsI	1.218	–	1.119	1.083	1.196
ZnS	0.427	0.193	0.459	1.541	0.821
CdS	0.473	0.278	0.378	1.685	0.879
PbS	0.305	–	0.481	0.998	–
ZnSe	–	–	0.474	1.876	1.259
ZnTe	–	–	–	0.563	1.095
CdTe	0.959	0.535	0.696	2.681	–
InP	–	0.114	0.467	–	–
GaSb	0.514	0.165	0.748	2.087	–
InSb	0.700	0.264	0.978	2.691	1.444
SiC	0.105	0.034	0.193	1.250	0.392
C (diamond)	0.065	0.018	–	1.866	0.311
Si	0.211	0.060	0.319	1.858	0.533
Ge	0.379	0.106	–	2.069	0.902
BeO	0.100	–	0.170	0.776	0.334
MgO	0.145	0.074	0.215	0.825	0.490
CaO	–	–	–	–	–
Sc_2O_3	0.106	0.047	–	–	0.254
Y_2O_3	–	0.053	0.171	–	0.256
TiO_2 cub	–	0.066	0.274	1.077	0.346
tet.	0.162	0.049	0.207	0.801	0.259

of any of these quantities is expected and is observed (Fig. 9).

4.2.2. Thermodynamic data

If the transmission is plotted directly against the standard heat of formation of the crystalline compound, a well-defined peak is obtained centred around $-\Delta H_f \sim 320\,kJ\,mol^{-1}$ (Fig. 10). The transmission increases sharply in the range $-\Delta H_f \sim 480$ to $320\,kJ\,mol^{-1}$, whilst for $-\Delta H_f \gtrsim 480\,kJ\,mol^{-1}$ little change is apparent, although the scatter of data is large. For $-\Delta H_f \lesssim 320\,kJ\,mol^{-1}$ transmission again decreases and this is noted for CdS, CdTe and AgCl. From bond-strength considerations, it would be expected that the greater the heat of formation of a compound, the lower the infra-red transmission.

In addition to optical effects, lattice vibrations are also responsible for the thermal properties of a solid, and hence some degree of correlation between infra-red transmission and heat capacity may be expected. If transmission is plotted

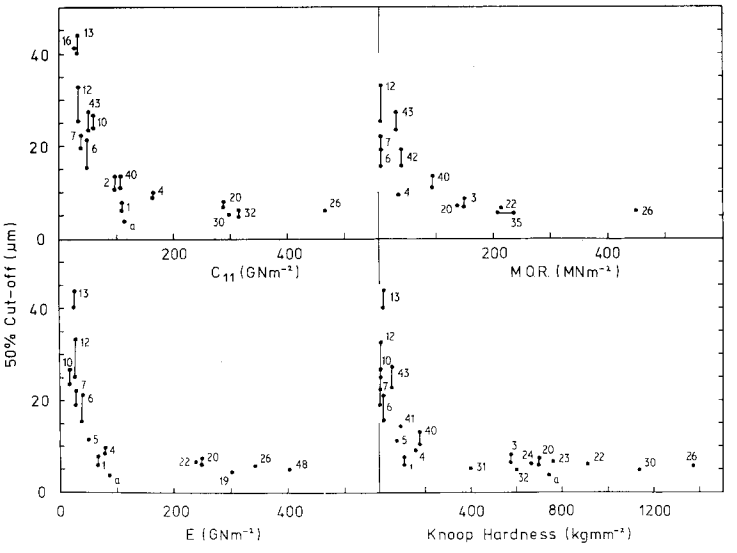

Figure 9 Relationship between 50% infra-red cut-off and C_{11}, E, MOR, and knoop hardness of various materials.

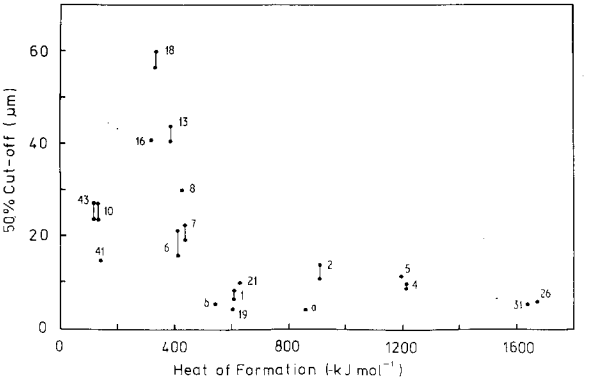

Figure 10 The 50% infra-red cut-off as a function of the heat of formation of various crystalline compounds

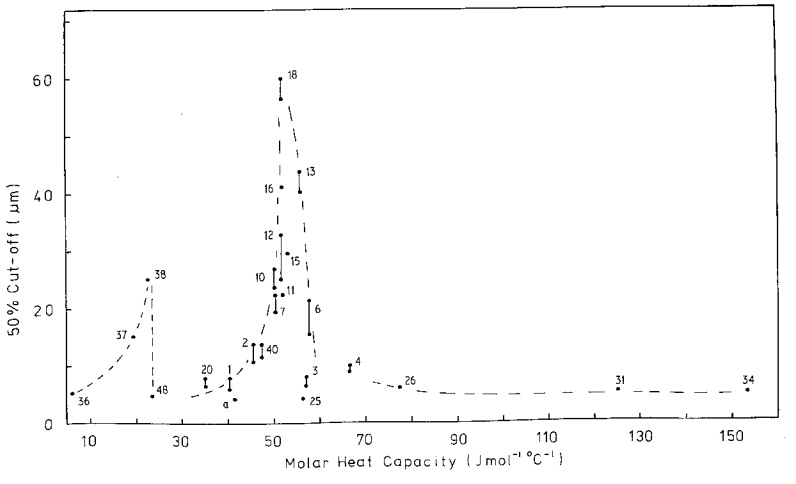

Figure 11 Variation of 50% infra-red cut-off with molar heat capacity.

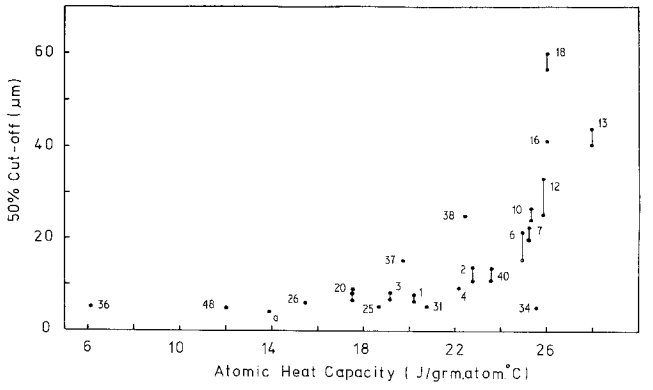

Figure 12 Variation of the 50% infra-red cut-off with the atomic heat capacity.

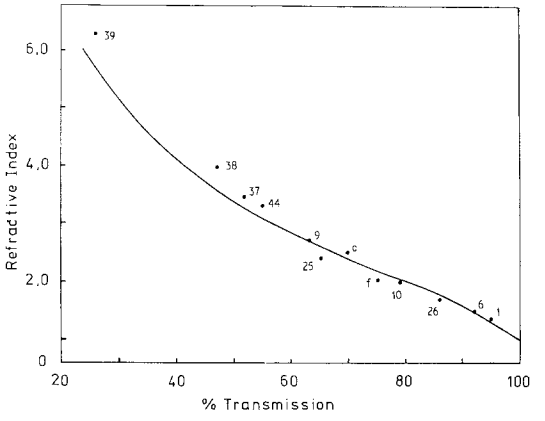

Figure 13 Refractive index versus the expected % transmission, assuming plane parallel-faced samples, and neglecting absorption losses.

directly against heat capacity, a very general trend of increasing transmission with decreasing heat capacity is observed. However, when transmission is plotted against the molar heat capacity, two sharply defined peaks in transmission are found, one associated with elemental homopolar materials centred around 10 to 25 $J\,mol^{-1}\,°C^{-1}$ and the other associated with highly or moderately ionic materials centred around 50 to 55 $J\,mol^{-1}\,°C^{-1}$ (Fig. 11).

The reason for sharply defined peaks in transmission at certain values of molar heat capacity is not too clear, although if the *atomic* heat capacity (defined as the heat absorbed per atom of substance), is employed, we note only a gradual decrease in transmission with decreasing atomic heat capacity (Fig. 12).

4.3. Prediction of reflection losses

Reflection losses at two interfaces, assuming a plane parallel-faced sample, and neglecting absorption losses, may be estimated from the relationship:

$$\text{Transmission} \sim (1-R)^2 \qquad (14)$$

where R is the reflectivity per interface given by Equation 4. Reference to Fig. 13 illustrates that

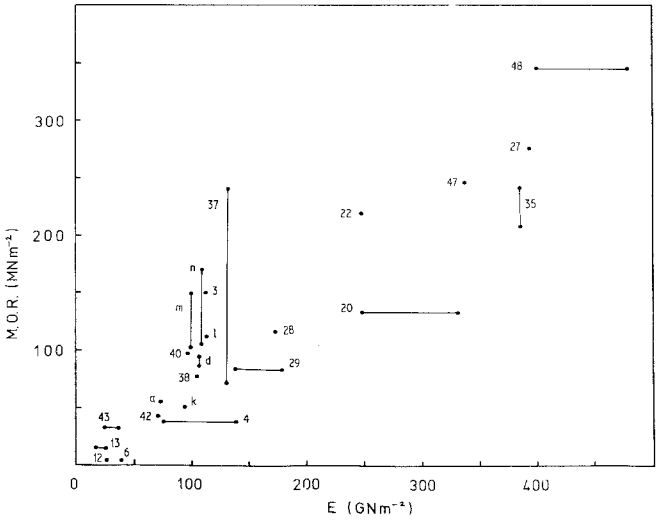

Figure 14 Relationship between MOR and E of various ceramic and glass materials.

this approximation is quite satisfactory, although at high values of n ($\gtrsim 2.8$) transmission is generally slightly greater than predicted.

4.4. Prediction of short wavelength cut-on

The value of the short wavelength cut-on is very dependent on the homogeneity and purity of the material. A comparison of the cut-on for 10% transmission with the theoretically derived value employing Equation 7 is summarized in Table VI where it is noted that the values usually agree to within about 10%.

4.5. General prediction of mechanical properties: modulus of rupture

Although the modulus of rupture of brittle materials is highly dependent on the surface condition of the sample, and also the majority of tests that have been carried out are in no way adequately standardized, a trend of increasing MOR with increasing E is apparent (Fig. 14). The data are shown within the limits reported, and in many cases the scatter is quite large, but the relationship is apparent.

The fact that MOR does generally increase with E, and also that infra-red transmission is related to E, increasing as E decreases, has important implications, suggesting that any strengthening mechanism which relies on an increase in E for the bulk material will most probably lead to a reduction in infra-red transmission. Hence, the most appropriate technique for strengthening materials will be surface methods, or bulk methods which increase the strain to failure and do not substantially alter the value of E.

4.6. New materials

New materials may be drawn from the oxides and other chalcogenides, the halides or the carbides, nitrides, borides, silicides or germanides, and, in general, must be of cubic symmetry, unless the anisotropy in refractive index is very small. Depending on the application, and as outlined earlier, a considerable degree of compromise may be necessary in terms of mechanical and physico-chemical properties, ease of fabrication, and infra-red transmission. The most promising materials may include certain oxides and fluorides, there being very few viable candidates from the remaining groups, and these will be discussed in detail in a later paper.

TABLE VI Electronic energy gap and cut-on wavelength of various materials.

Material	E_g (eV)	Cut-on (μm)	Approximate experimental cut-on (10% for $t = 2$ mm)
Elements			
C	5.4	0.230	0.25
Si	1.15	1.078	1.2
Ge	0.65	1.908	1.8
Sn	0.08	15.500	–
am Se	1.6	0.775	1.0
Te	0.33	3.758	3.5
III–V compounds			
BP	6.0	0.207	–
AlP	2.5	0.496	–
AlAs	2.3	0.539	–
AlSb	1.52	0.816	–
GaP	2.25	0.551	0.6
GaAs	1.35	0.919	1.0
GaSb	0.69	1.797	–
InP	1.27	0.976	1.0
InAs	0.35	3.543	3.8
InSb	0.17	7.294	7.5
IV–VI compounds			
PbS	0.37	3.351	–
PbSe	0.26	4.769	5.0
PbTe	0.25	4.960	5.0
II–VI compounds			
ZnS	3.65	0.340	0.4
ZnSe	2.6	0.477	0.5
ZnTe	2.15	0.577	–
CdS	2.4	0.517	0.5
CdSe	1.74	0.713	–
CdTe	1.50	0.827	0.9
HgS	2.5	0.496	–
HgSe	0.3	4.133	–
HgTe	0.2	6.200	–
Oxides			
MgO	7.3	0.170	0.25
CaO	6–7	0.21–0.18	0.28
Ga_2O_3	4.4	0.282	–
In_2O_3	~2.8	0.443	–
Miscellaneous			
SiC	3.0	0.413	–
BN	~4	0.31	–
CuBr	2.94	0.422	–
$MgSi_2$	0.77	1.610	–

5. Conclusions

(1) The long wavelength cut-off for many cubic binary polar materials, in addition to some homo-

polar, complex, or non-cubic materials, may be estimated to within ~16% using the simple diatomic oscillator model and replacing the force constant by $C_{xy}a$, where C_{xy} and a are the largest elastic constant and lattice parameter, respectively. The prediction generally becomes less accurate for: (a) polycrystalline materials, and (b) if C_{xy} tends towards the value of the next highest elastic constant. The value of C_{xy} may be substituted by E, hardness, or melting point to yield qualitative predictions of infra-red transmission.

(2) Maximum infra-red transmission is obtained with non-elemental materials for which the standard heat of formation and the molar heat capacity are centred around $-320\,\mathrm{kJ\,mol^{-1}}$ and 50 to $55\,\mathrm{J\,mol^{-1}\,°C^{-1}}$, respectively.

(3) Any improvement in the mechanical properties of existing infra-red materials should ideally be achieved by increasing the strain to failure of the material rather than by relying on an increase in E, and surface techniques are the most promising for accomplishing this. Application of thicker abrasion resistant coatings may also be feasible by the techniques of CVD or plasma-spraying.

(4) Growth of large single crystals is limited by practical difficulties to small sizes and simple shapes, with the possible exception of the modified capillary Czochralski method, and polycrystalline materials are limited by the requirement for ultra-pure starting materials when prepared by hot-pressing or sintering. The technique of CVD has been successfully used in the production of complex shapes for a limited number of materials, and may prove a useful research area.

(5) Currently, the most useful polycrystalline materials which exhibit a combination of desirable properties including good infra-red transmission to at least 5 μm, are certain Group III and rare earth oxides, MgO, $MgAl_2O_4$, $LiAl_5O_8$, Al_2O_3, MgF_2, ZnS and ZnSe.

Acknowledgements

The authors are grateful to the Ministry of Defence, Procurement Executive, for financial support. We also wish to thank Eastman Kodak, Texas Instruments, Harshaw Chemicals and GEC (USA) for supplying technical information on commercial products.

References

1. G. HASS and J. E. WAYLONIS, *J. Opt. Soc. Amer.* **50** (1960) 1133.
2. E. B. WILSON, J. C. DECIUS and P. C. CROSS, "Molecular Vibrations" (McGraw-Hill, New York, 1955).
3. J. N. HODGSON, "Optical absorption and dispersion in solids" (Chapman and Hall, London, 1970).
4. J. K. D. MACKENZIE, *J. Amer. Ceram. Soc.* **55** (1972) 68.
5. M. P. O'HORO, A. L. FRISILLO and W. B. WHITE, *J. Phys. Chem. Solids* **34** (1973) 23.
6. I. W. DONALD and P. W. McMILLAN, *J. Mater. Sci.* **11** (1976) 949.
7. H. S. PEISER, editor, Proceedings of the International conference on Crystal growth, Boston, 1966 (Pergamon Press, Oxford, 1967).
8. H. E. LaBELLE, *Mater. Res. Bull.* **6** (1971) 581.
9. J. JORGENSEN and R. C. ANDERSON, *J. Amer. Ceram. Soc.* **50** (1967), 553.
10. C. GRESKOVICH and K. N. WOODS, *Amer. Ceram. Soc. Bull.* **52** (1973) 473.
11. E. CARNALL and D. PEARLMAN, *Mater. Res. Bull.* **7** (1972) 647.
12. K. S. MAZDIYASNI, C. T. LYNCH and J. S. SMITH, *J. Amer. Ceram. Soc.* **48** (1965) 372.
13. B. J. MULDER, *Amer. Ceram. Soc. Bull.* **49** (1970) 990.
14. Y. S. KIM and F. R. MONFORTE, *ibid.* **50** (1971) 532.
15. R. A. JAEGER and T. J. MILLER, *ibid.* **53** (1974) 858.
16. V. VORA and P. R. ZUPP, *Mater. Res. Bull.* **5** (1970) 977.
17. J. R. BOOTH, W. D. KINGERY and H. K. BOWEN, *J. Cryst. Growth* **29** (1975) 257.
18. K. A. WICKERSHEIM and R. A. LEFEVER, *J. Opt. Soc. Amer.* **51** (1961) 1147.
19. J. J. RUBIN and L. G. VAN UITERT, *Mater. Res. Bull.* **1** (1966) 211.
20. F. GALASSO, and W. DARBY, *J. Opt. Soc. Amer.* **55** (1965) 332.
21. W. A. BONNER and L. G. VAN UITERT, *Mater. Res. Bull.* **2** (1967) 131.
22. R. J. BAUGHMAN and R. A. LEFEVER, *ibid.* **3** (1968) 457.
23. G. ZYDIK, *ibid.* **10** (1975) 9.
24. R. FALCKENBERG and H. WORL, *ibid.* **9** (1974) 519.
25. L. G. VAN UITERT, W. H. GRODKIEWICZ and E. F. DEARBORN, *J. Amer. Ceram. Sco.* **48** (1965) 105.
26. H. M. DESS, "YAG Crystals", Report No. 1, US Army Electronics Command, Fort Monmouth, AD 624 596 (1965).
27. C. MACNEILL, *J. Opt. Soc. Amer.* **53** (1963) 398.
28. J. B. MOONEY, *Infra-red Physics* **6** (1966) 153.
29. E. F. YOUNG and C. H. PERRY, *J. Appl. Phys.* **38** (1967) 4624.

30. A. L. GENTILE and O. M. STAFSUDD, *Mater. Res. Bull.* **9** (1974) 105.
31. C. O. DUGGER, *ibid.* **9** (1974) 331.
32. P. J. GIELISSE, S. S. MITRA, J. N. PLENDL, R. D. GRIFFIS, L. C. MANSURI, R. MARSHALL and E. A. PASCOE, *Phys. Rev.* **155** (1967) 1039.
33. K. S. MAZDIYASNI, C. T. LYNCH and J. S. SMITH, *J. Amer. Ceram. Soc.* **50** (1967) 532.
34. P. J. JORGENSEN and R. C. ANDERSON, *ibid.* **50** (1967) 553.
35. C. GRESKOVICH and K. N. WOODS, *Amer. Ceram. Soc. Bull.* **52** (1973) 473.
36. R. J. BRATTON, *J. Amer. Ceram. Soc.* **57** (1974) 283.
37. M. MIYAUCHI and G. TODA, *ibid.* **58** (1975) 157.
38. S. K. DUTTA and G. E. GAZZA, *Mater. Res. Bull.* 4 (1969) 791.
39. R. A. LEFEVER and J. MATSKO, *ibid.* **2** (1967) 865.
40. G. E. GAZZA, D. RODERICK and B. LEVINE, *J. Mater. Sci.* **6** (1971) 1137.
41. E. CARNALL and D. PEARLMAN, *Mater. Res. Bull.* 7 (1972) 647.
42. T. K. GUPTA, B. R. ROSSING and W. B. STRAUB, *J. Amer. Ceram. Soc.* **56** (1973) 339.
43. T. K. GUPTA, private communication (1976).
44. R. W. RICE, *J. Amer. Ceram. Soc.* **50** (1969) 420.
45. E. CARNALL, *Mater. Res. Bull.* **2** (1967) 1075.
46. G. E. GAZZA, *J. Amer. Ceram. Soc.* **55** (1972) 172.
47. G. H. HAERTLING, *Amer. Ceram. Soc. Bull.* **49** (1970) 564.
48. G. H. HAERTLING and L. E. LAND, *J. Amer. Ceram. Soc.* **54** (1971) 1.
49. F. W. AINGER, D. APPLEBY and C. J. KIRKBY, *J. Mater. Sci.* 8 (1973) 1825.
50. I. MATSUYAMA and S. JYOMURA, *J. Amer. Ceram. Soc.* **58** (1975).
51. K. MIYAUCHI and G. TODA, *ibid.* **58** (1975) 361.
52. S. K. DUTTA and R. M. SPRIGGS, *Mater. Res. Bull.* 4 (1969) 797.
53. K. KODAIRA and M. KOIZUMI, *ibid.* **6** (1971) 261.
54. B. E. YOLDAS, *Amer. Ceram. Soc. Bull.* **54** (1975) 286.
55. R. R. SMYTH and J. P. ROBERTS, "Fabrication of transparent ceramics", Progress reports 1 and 2, Deptartment of Ceramics. University of Leeds (1965).
56. M. J. LATIMER, A. J. WHITEHEAD, J. B. HUFFADINE and N. C. MOORE, "Magnesium Fluoride Summary Report, October 1960–June 1969", Plessey Co.
57. L. S. LADD, *Infra-red Physics* **6** (1966) 145.
58. B. A. DIBENEDETTO and J. PAPPIS, "Chemical Vapor deposition of multispectral domes", Raytheon Co., AD-A014 362, April 1975.
59. K. NIIHARA and T. HIRAI, *J. Mater. Sci.* **11** (1976) 593.
60. C. D. SALZBERG, *J. Opt. Soc. Amer.* **51** (1961) 1149.
61. V. P. OPPENHEIM and V. EVEN, *ibid.* **52** (1962) 1078.
62. D. A. GRYUNAK and D. E. BURCH, *ibid.* **55** (1965) 625.
63. V. P. OPPENHEIM and A. GOLDMAN, *ibid.* **54** (1964) 127.
64. D. T. GILLESPIE, A. L. OLSEN and L. W. NICHOLS, "Transmittance of optical materials at high temperatures in the 1–12 μm range", NAVWEPS Rep. 8558, October 1964, AD 609 036.
65. A. G. EVANS and H. JOHNSON, *J. Amer. Ceram. Soc.* **58** (1975) 244.
66. S. W. FEIMAN, J. J. MECHOLSKY, R. W. RICE and J. C. WURST, *ibid.* **58** (1975) 406.
67. J. D. WALTON, *Amer. Ceram. Soc. Bull.* **53** (1974) 225.
68. M. COENEN, M. FUALSTICH and F. REITMAYER, Second International Symposium on Electromagnetic Windows, Paris (1971) p. 487.
69. G. Y. CHIN, L. G. VAN UITERT, M. L. GREEN, G. J. ZYAZIK and T. Y. KOMETANI, *J. Amer. Ceram. Soc.* **55** (1973) 369.
70. A. L. RUOFF and C. U. S. N. RAO, *ibid.* **58** (1975) 503.
71. F. BUCH and C. N. AHLQUIST, *Mater. Sci. Eng.* **13** (1974) 194.
72. J. A. BATT, F. C. DOUGLAS and F. S. GALASSO, *Amer. Ceram. Soc. Bull.* **48** (1969) 622.
73. J. J. KROCHMAL, Proceedings of the Symposium on Electromagnetic Windows. Vol. 1, June 1968, AD 841 562.
74. H. P. KIRCHNER, *J. Canadian Ceram. Soc.* **40** (1971) 15.
75. H. P. KIRCHNER and R. M. GRUVER, *Mater. Sci. Eng.* **13** (1974) 63.
76. H. P. KIRCHNER, W. A. SOTTER and R. M. GRUVER, *J. Amer. Ceram. Soc.* **58** (1975) 353.
77. J. E. DOHERTY, J. G. TSCHINKEL and S. M. COPLEY, *Amer. Ceram. Soc. Bull.* **52** (1973) 681.
78. M. MILER, *Infra-red Physics* 7 (1967) 117.
79. E. L. CHURCH, S. R. NAGAL, S. E. SCHNATTERLY and T. N. TUDRON, *Appl. Optics* **13** (1974) 1274.

Received 1 October and accepted 28 October 1977.